03,07

Effect of vacuum annealing on local radial magnetization of PrDy−FeCo−B microwires

© E.V. Dvoretskaya[1,2], R.B. Morgunov[1,2]

[1] Federal Research Center of Problems of Chemical Physics and Medicinal Chemistry RAS, Chernogolovka, Russia
[2] All-Russian Scientific Research Institute of Aviation Materials of the Research Center „Kurchatov Institute“, Moscow, Russia

E-mail: Dvoretskaya95@yandex.ru

Received October 28, 2024
Revised November 29, 2024
Accepted December 7, 2024

A new type of microcombs (microstructures with alternating magnetization zones) based on microwires in which the magnetization periodicity is caused by equidistant alternation of natural domains is proposed. The presence of quasi-periodic radial magnetization and the effect of temperature and magnetic field on the magnetic relief in PrDy−FeCo−B microwires are established. Analysis of the chemical, phase and structural composition of the microwires revealed the necessary conditions for creating a periodic magnetic relief. It is established that annealing affects the magnetic relief and changes the structure of initially amorphous microwires.

Keywords: microstructures, amorphous, rare earth, radial domains, magnetic domain structure, microcombs.

DOI: 10.61011/PSS.2025.01.60595.285

1. Introduction

Magnetic micro-combs (microstructures with alternating magnetization zones) are necessary in micro robotics, MEMS technologies, actuators and magnetic flux analyzers. Typically, magnetic micro-combs are artificial linear magnets of periodic shape. Linear periodic magnetic structures are widely in demand in the modern industry of micro devices and microelectromechanical systems (MEMS) [1,2]. The simplest example of their application is an actuator that ensures a linear displacement of a ferromagnetic core in a periodic magnetic field [3–5]. The manufacture of an electromagnetic micro-comb drive for a different number of magnetized zones is demonstrated in Ref. [6]. It has been shown that the field generated by such an object significantly reduces the current consumption by 60% and linearizes the current-displacement characteristic for small offsets up to $50\,\mu$m in actuators [6]. This behavior was predicted by modeling, and it was also shown that the improvement of devices based on micro-combs is limited by the saturation field of the material [7]. High-performance electromagnetic microactuators can be designed and manufactured without mold designing and lithography owing to the spontaneous formation of a domain structure.

Another well-known application of magnetic ridges is the separation of magnetic nanoparticles moving with the flow of biological fluid in a microfluidic chip [8,9]. The separation of specific cells or molecules in multicomponent fluids is a key function required for MEMS technologies used in biomedical applications. A micro-comb with a highly gradient magnetic field can be inserted into a microfluidic capillary. When the magnetic micro-comb is magnetized, the magnetic particles can be removed from the flux and transferred to a separate reservoir. Continuous separation of the mixture components directly on a micro-comb in a periodic magnetic field can simplify the operation of the microsystem and potentially increase the separation efficiency. In particular, microfluidic systems can be used in micromagnetic analyzers to continuously separate components from flowing liquids. Continuous separation of magnetic particles in microfluidic channels has been demonstrated in a microsystem equipped with a magnetic comb [6,8].

The need to implement the above break devices on a microscale requires microstructures with periodic magnetization distribution. Thin ferromagnetic microwires with a periodically varying (modulated) diameter are usually fabricated to meet these conditions. Another possible way to create magnetic micro-combs is to study the natural distribution of magnetization along microwires with periodically distributed magnetic domains [10]. Microwires with periodic magnetization generated by radial magnetic domains are described in Refs. [10–14]. The spontaneous periodic distribution of magnetization depends on the crystal structure, phase and chemical composition, as well as the geometry of the microwires. This distribution can be controlled by heat treatment and an external magnetic field.

This study is aimed at identifying correlations between the structural and phase composition of microwires and the structure of magnetic radial domains, as well as the distribution of the magnetic field in the periodic domain structure along the microwire PrDy−FeCo−B.

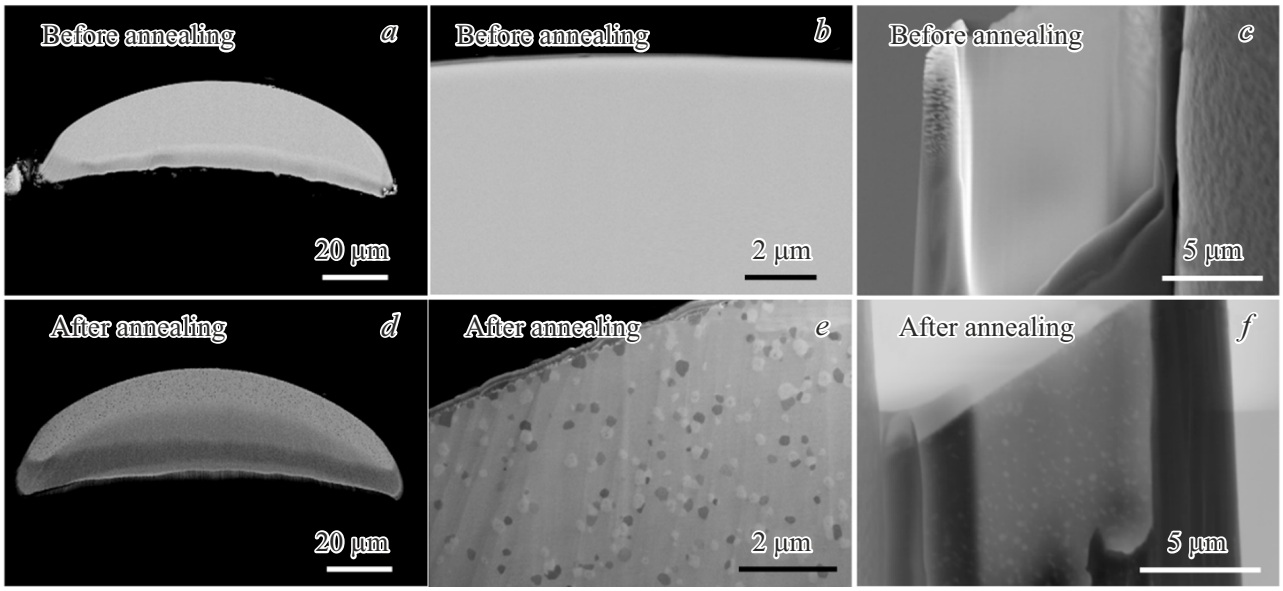

Figure 1. SEM-images of polished ends of microwires before (a, b) and after (d, e) vacuum annealing. SEM images of lamellae cut from microwires before (c) and after (f) annealing.

2. Samples and experimental methods

PrDy−FeCo−B microwires were obtained by extraction of a hanging melt droplet (initial droplet composition $Pr_{3.5}Dy_6Fe_{49}Co_{40}B_{2.5}$) [13]. The composition of the microwire is homogeneous throughout the entire volume of the sample, which was previously established by mapping chemical elements, energy dispersive X-ray spectroscopy (EDX) [10,12–14]. Two types of samples were used in the experiments: the initial amorphous microwires (microwire 1) (Figure 1, $a-c$) and the same microwires after vacuum (10^{-5} Torr) annealing (microwire 2) during 2 h at 700°C (Figure 1, $d-f$).

SEM images, mapping of chemical elements, and energy dispersive X-ray spectroscopy (EDX) at the end of the microwires were obtained using a TESCAN CLARA ultra-high resolution scanning electron microscope. The cross-section and polishing of the ends of the micro-wires (Figure 1, a, b, d, e) were performed using Technoorg Linda SEMPrep2 ion etching and ion polishing unit (cutting and polishing of the ends of the micro-wires with ions Ar^+ took 2.5 h).

The lamellae of the microwires before and after vacuum annealing (Figure 1, c, f) were fabricated and analyzed using TESCAN AMBER FIB-SEM microscope (the lamellae were cut by Ga^+ ions). FIB-SEM had Oxford Ultim EDX spectrometer for phase analysis, Oxford EBSD detector, and AZtec software.

The magnetic moment of the microwires was measured using MPMX 5XL Quantum Design SQUID magnetometer. The magnetic domains were visualized and the samples were remagnetized using the MOIF (Magneto-Optical Indicator Film) method described in Ref. [15]. The MOIF method is based on the magneto-optical Faraday effect, which consists in rotating the plane of polarization of linearly polarized light as it passes through an optically active substance deposited on the surface of a microwire and located in its magnetic scattering field.

3. Experimental results and discussions

3.1. Chemical and phase composition of microwires

The SEM images of the surface of the polished end face and the lamella of the microwire after vacuum annealing exhibit a large number of inclusions (Figure 1, e, f). Such features are not observed on the surface of the microwire section before vacuum annealing (Figure 1, b, c). Figure 2, a and b show SEM images and distribution maps of chemical elements at the ends of microwires before and after vacuum annealing, respectively.

The distribution of chemical elements at the ends of microwires 1 and 2 is homogeneous. The EDX analysis of ends of microwires 1 and 2 was conducted to analyze the differences in the chemical and phase composition of microwires 1 and 2 (Figure 3, a, b, respectively). It can be seen that the EDX spectra of microwires are different before and after vacuum annealing. This can be explained by a change of the phase composition of the sample under the impact of high temperatures.

The lamellae (Figure 1, c, f) of the microwires 1 and 2 were analyzed to obtain additional information about the structure of the samples. Figure 4 shows SEM images of lamellae of microwires 1 and 2 in different scanning modes. The matrix of microwire 1 looks fine-grained, but it was

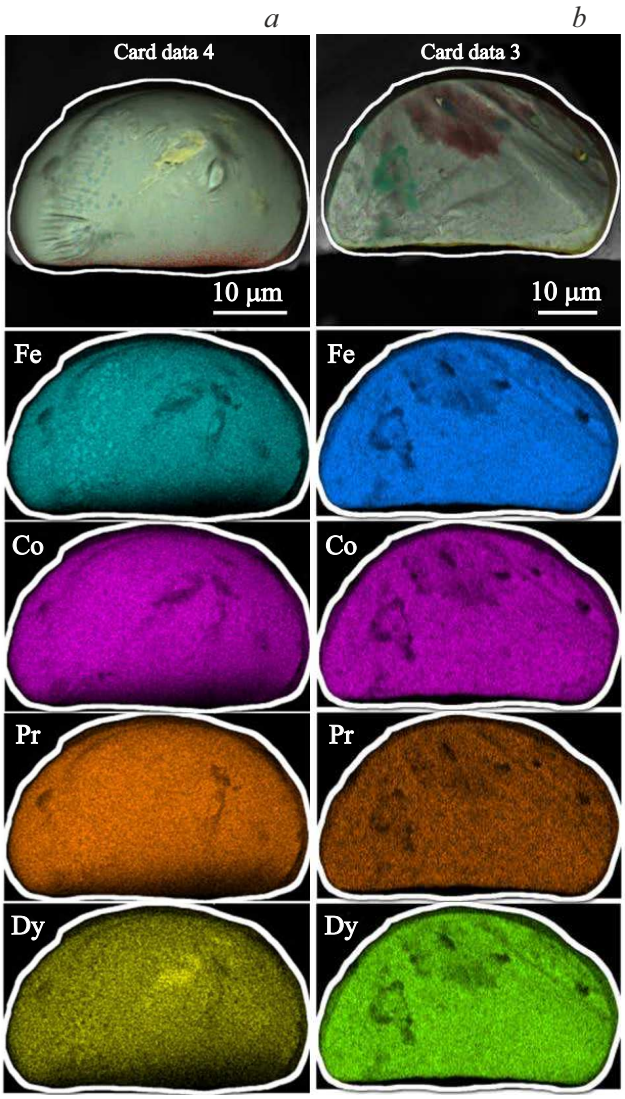

Figure 2. SEM-images of the end of the microwire before (a) and after (b) vacuum annealing and corresponding distribution maps of the basic chemical elements (Fe, Co, Pr, Dy) composing the microwire.

not possible to identify the phases using TESCAN AMBER FIB-SEM microscope, that is, microwire 1 is completely amorphous from the point of view of this method. Since the Kikuchi figures were not formed before vacuum annealing in microwire 1, the structure shown in Figure 4, a refers to the amorphous state of the microwire. Small heterogeneities in the figure, therefore, characterize not small crystallites, but a heterogeneous amorphous state.

The electron diagram of the microwire after vacuum annealing (Figure 5, b) shows a large number of point reflexes and the disappearance of the amorphous halo characteristic of the microwire before vacuum annealing (Figure 5, a). Electron diffraction patterns of microwire 1 before vacuum annealing and microwire 2 after annealing were typical.

A crystallographic group of the crystal structure of microwire 2 was identified by constructing a family of Kikuchi bands and the type of its orientation at each point of the sample surface was determined (Figure 6). EDX (allowing recording the chemical composition) and EBSD (Electron BackScatter Diffraction, which allows determining the crystallographic group of a local area, its orientation at each point of the sample surface) detectors in FIB-SEM TESCAN AMBER microscope were used simultaneously for phase identification. Detected electron beams (diffraction patterns) correspond to certain families of crystal planes. The three-dimensional crystallographic orientation of the studied lamella area is determined automatically based on the position and relative orientation of the Kikuchi bands by comparing the obtained Kikuchi pattern with theoretical data on the corresponding crystalline phase. Then, the phase identification process is conducted based on the chemical composition data and on the basis of crystallographic data. The presence of Kikuchi bands, the angles of their mutual intersection, and the thickness of the bands depend on the observed spatial group of the crystal structure and the orientation of the crystal structure. It was not possible to record Kikuchi patterns in microwire 1 before vacuum annealing. Kikuchi patterns are not formed in microwire 1 before vacuum annealing, which indicates the amorphous structure of the sample.

Figure 7, a shows the phase maps of the sample of the lamella of microwire 2. Areas where the indexing module cannot index the Kikuchi band family correctly (for example, deformed areas, grain boundaries, scratches) usually look darker on the map. Phase maps allow seeing the phase distribution. Each phase in the dataset has its own color. The pink color corresponds to the tetragonal phase 2-14-1, the blue color corresponds to the bulk-centered cubic phase BCC, and the black color corresponds to the area of the unidentified phase. Regions with a bulk-centered cubic Fe lattice (Figure 7, a, pink color) and regions with a tetragonal lattice 2-14-1 (Figure 7, a, blue color) were identified in the lamella of microwire 2, wherein Fe atoms can be partially replaced by Co atoms in both lattices, and Pr atoms can be partially replaced by Dy atoms. The non-indexed regions (black) have a crystalline structure and families of Kikuchi bands have been recorded. However, it was impossible to determine which phase they correspond to, as the necessary information is missing from the embedded database, and these areas remain unindexed. Figure 7, b shows a map of the inverse pole figures (IPF).

The maps of the inverse pole figures show the crystallographic orientation of the crystal lattice in each grain (Figure 7, b) and give an idea of the misorientation of the crystallographic axes and the main axes of magnetization of the crystallites (grains) of the microwire 2.

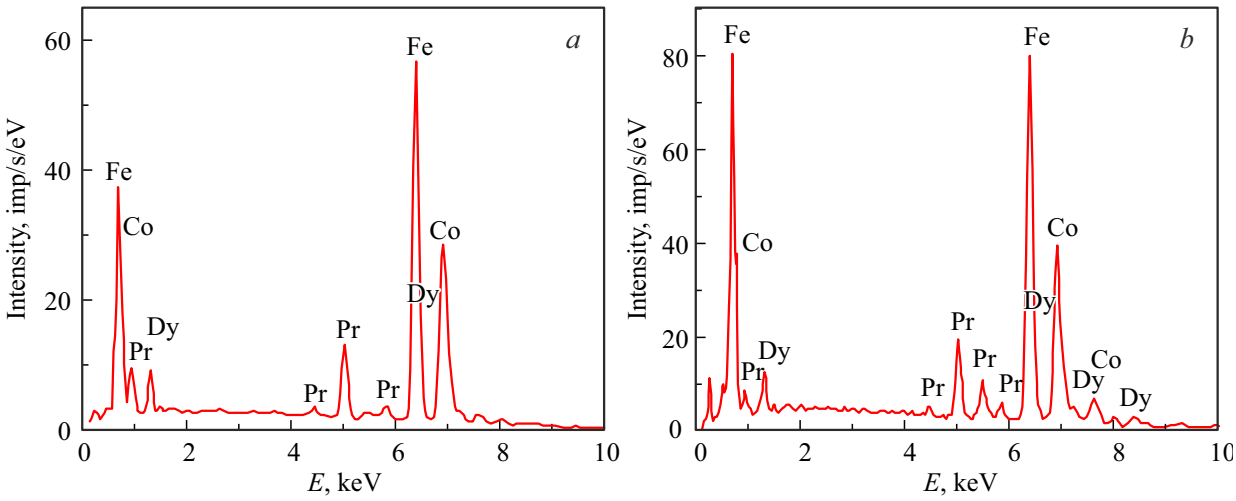

Figure 3. EDX spectra of the end of the microwire before (*a*) and after (*b*) vacuum annealing.

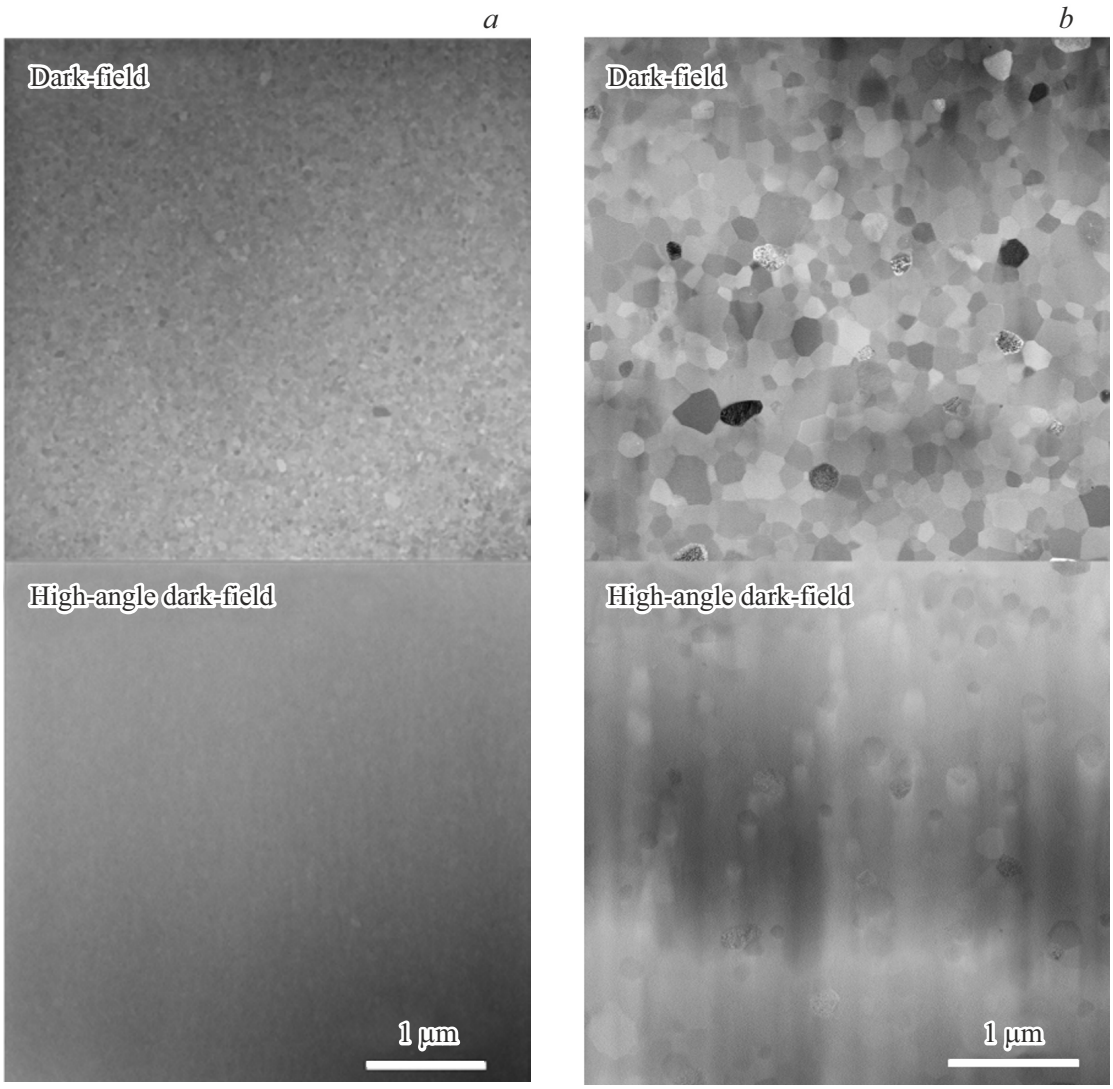

Figure 4. SEM images of the microwire lamella before (*a*) and after (*b*) annealing.

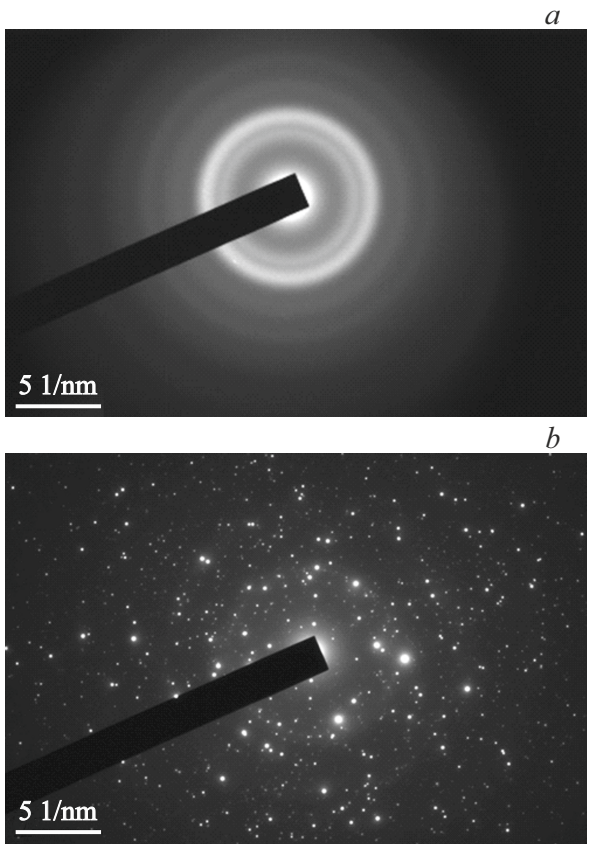

Figure 5. Diffraction patterns for lamellae of amorphous microwire (a) and microwire after vacuum annealing (b).

3.2. Magnetic properties of microwires before and after vacuum annealing

Microwires 1 and 2 significantly differ in their magnetic properties. Figure 8, *a, b* shows the hysteresis loops of an amorphous microwire 1 before annealing and the same polycrystalline microwire 2 after vacuum annealing at 700°C, respectively.

Amorphous microwires (Figure 8, a) are characterized by a narrow ~ 8 Oe rectangular hysteresis loop with saturation in weak fields ~ 150 Oe. Vacuum annealing causes a significant increase of the coercive force from 8 Oe for amorphous microwires (Figure 8, a) to 10 kOe (Figure 8, b) for polycrystalline microwires in which the magnetization is not it reaches saturation even in the fields ~ 50 kOe. The stepwise shape of the hysteresis loop (Figure 8, b and Figure 9) indicates the presence of two phases simultaneously in polycrystalline microwires: a magnetically rigid, high-coercive phase 2-14-1 and a magnetically soft phase.

The model of two independent hystereses described in Ref. [16] allows for a simultaneous identification of the contributions of magnetically rigid and magnetically soft phases, which correspond to the indices $i = 1$ and $i = 2$ in case of expansion of the hysteresis loop of an annealed microwire 2:

$$m(H) = \sum_{i=1}^{2} \left[m_S^i - 2m_S^i / \left(1 + \exp((H \pm H_C^i)/p^i)\right) \right], \quad (1)$$

where $m(H)$ — magnetic moment, m_S^i — magnetic moment of saturation of the soft and hard phases, H — external field, signs „+“ and „–“ correspond to the descending and ascending parts of the loop, respectively, H_C^i — coercive fields of the magnetically soft and magnetically rigid phases, p^i — the squareness coefficient determined by $p^1 = 0.95$ for the magnetically rigid phase and $p^2 = 0.45$ for the magnetically soft phase.

Red lines in Figure 9 represent an approximation of the experimental data (gray symbols) with the expression (1), and the blue and green lines correspond to the rectangular component of the hysteresis loop obtained from the magnetically rigid phase and the inclined component — from the soft magnetic phase. The rectangular hysteresis loop (blue lines in Figure 9, a) is similar to the one observed in Ref. [17] for microwires containing Fe and B.

In addition to studying the integral magnetic moment, we also studied the distribution of the perpendicular component of magnetization along the microwire. Magneto-optical images of the domain structure of microwires before and after vacuum annealing were obtained using the MOIF (Magneto-Optical Indicator Films) method. The MOIF method made it possible to visualize the perpendicular component of the magnetization of the surface of a microwire and was not used to measure the magnetic characteristics of a microwire, such as $M(H)$, which does not affect the measurement error of magnetic characteristics in a SQUID magnetometer. Helmholtz coils were used as a magnetic field source, creating a uniform external field with a strength of up to 60 mT. The magnetization of the indicator film is in its plane in the absence of an external magnetic field, which makes it possible to visualize the scattering fields of the sample coated with the indicator film, deflecting the magnetization of the indicator film from its orientation along the axis of the microwire. Thus, the MOIF image shows dark and light areas with variable intensity corresponding to the areas of the sample with the magnetization component perpendicular to the surface of the microwire. MOIF images of the microwire before vacuum annealing are shown in Figure 10, a, and images of the microwire after annealing are shown in Figure 10, b under various external fields directed along the microwire.

Radial domains (alternating black and white zones) are observed in microwire 1 in the surface layer before vacuum annealing (Figure 10, a, Figure 11, a). The occurrence and appearance of the domain structure strongly depends on the magnitude of the external magnetic field. The intensity of the MOIF contrast increases with an increase of the strength of the external field, and a change in the direction of the lines of the external field leads to a change in the sign of the magnetization of the domains to the opposite. However, radial domains are not observed in the microwire 2 after

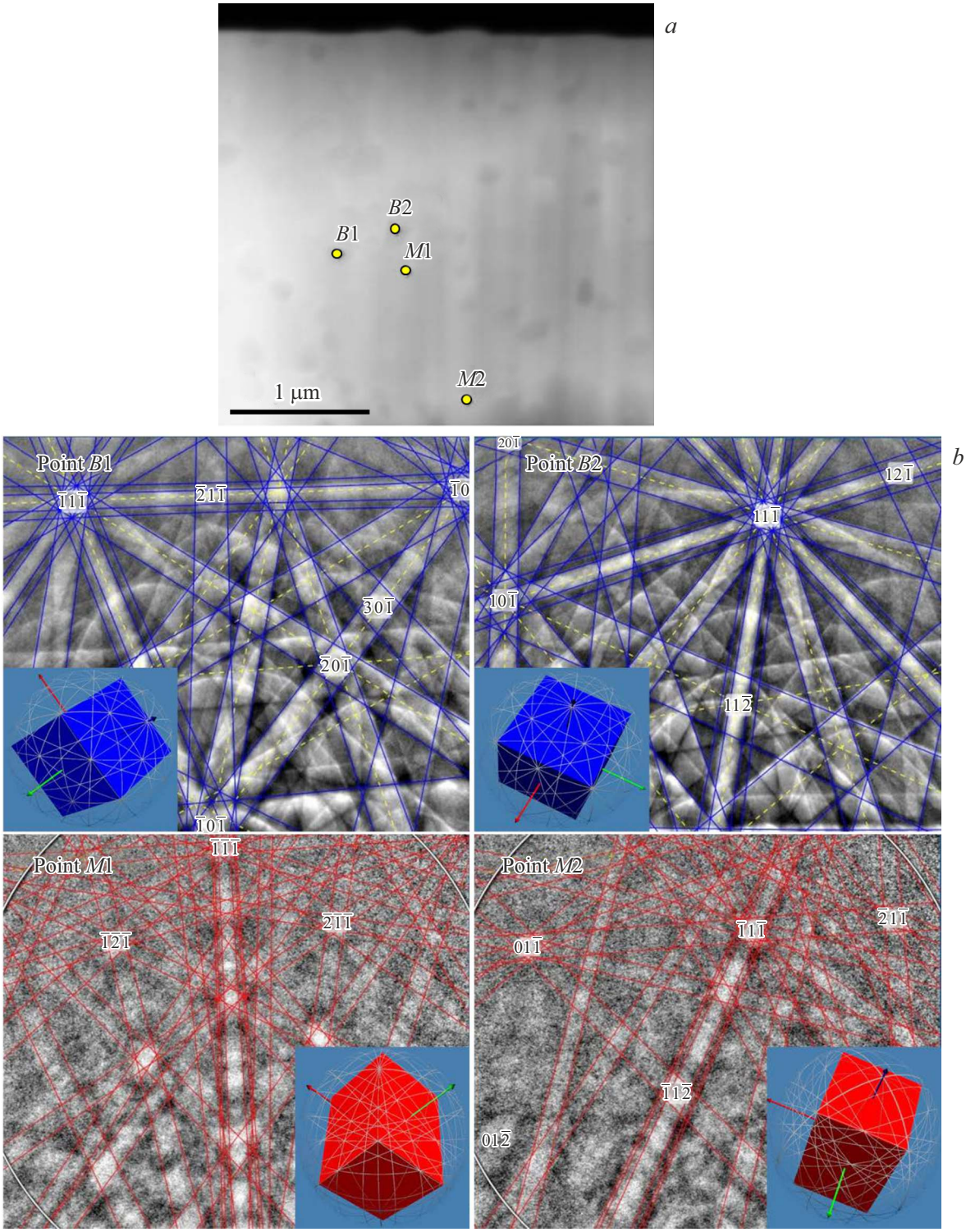

Figure 6. *a* — SEM image of a microwire 2 indicating the points at which Kikuchi patterns and their corresponding crystal phase orientations were recorded. *b* — Kikuchi patterns obtained in the area of inclusions (points B1 and B2). Kikuchi patterns obtained outside the area of inclusions (points M1 and M2).

vacuum annealing (Figure 10, *b*, Figure 11, *b*). At the same time, there are a large number of small, randomly located magnetic dipoles in the surface layers. The intensity and direction of the magnetization of the dipoles in the layers do not depend on the magnitude and direction of the external magnetic field. We attribute the presence of such magnetic features to the inclusions described in Section 3.1. The microwires turned out to be imperfectly cylindrical,

however, we can use the cylindrical microwire model, as in the works of [15,17]. At the same time, we understand that deviation from the cylindrical shape distorts the scattering

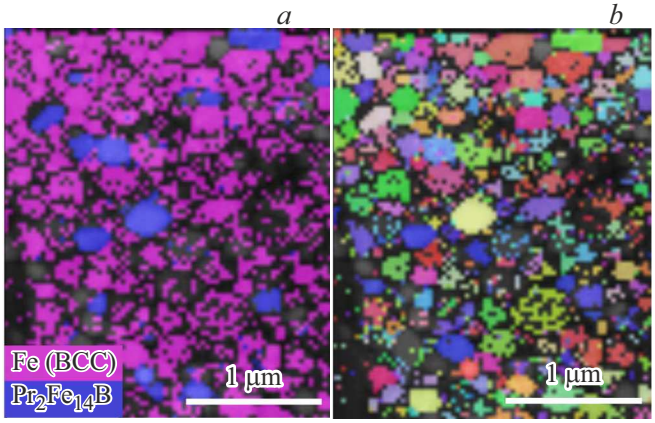

Figure 7. Phase map (a) and orientation map in the colors of the inverse pole figures (IPF) (b) for the microwire lamella after vacuum annealing.

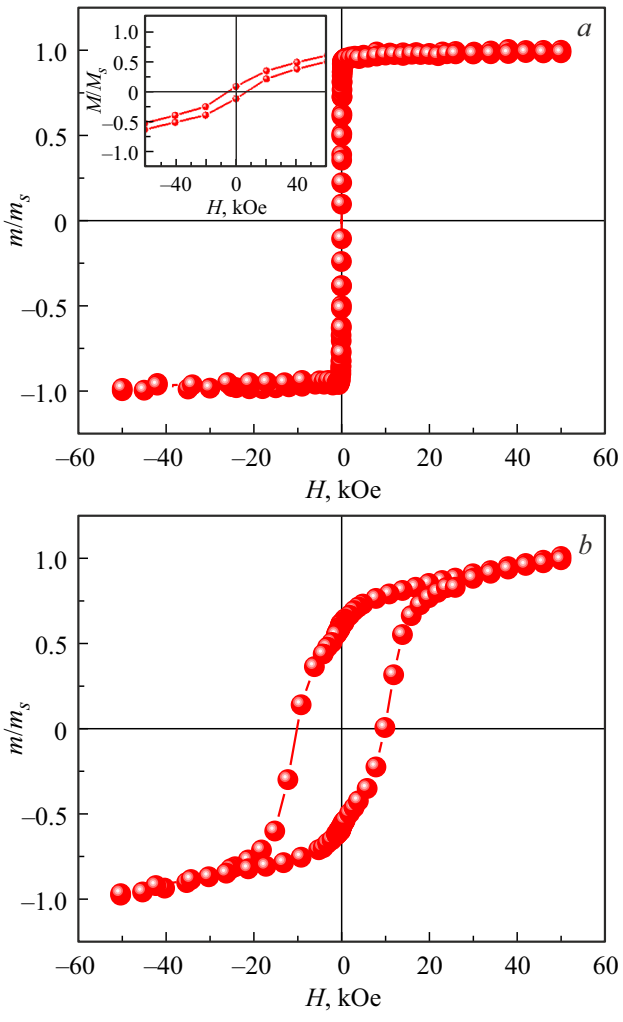

Figure 8. Hysteresis of the same microwire at 300 K before vacuum annealing (a) and after vacuum annealing (b).

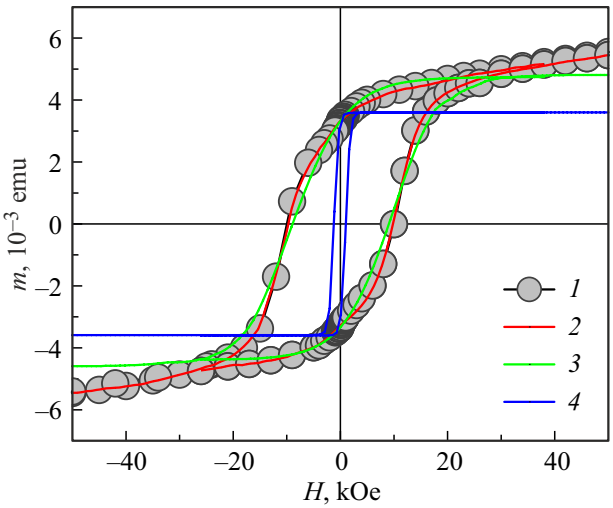

Figure 9. Microwire hysteresis at 300 K after vacuum annealing: *1* — experimental data; *2* — approximation by two hystereses. The individual magnetic contributions of the magnetically rigid high-coercive phase and the magnetically soft phase are shown by thin solid green (*3*) and blue (*4*) lines, respectively.

fields and magnetization inside the microwire, however, taking this factor into account becomes difficult, although it does not change the fundamental aspect of the discussions.

Radial heterogeneity is present in microwires before vacuum annealing, which may be associated with rapid cooling of the melt droplet (10^{-6} K). The temperature gradient is a source of mechanical stresses that are fixed in the wire, causing mechanically induced magnetic anisotropy along the radius of the micro-wire. The magnetostriction constant is of great importance within the framework of such a mechanism. Despite the absence of a glass shell in DyPr–FeCo–B microwires, a small gradient of mechanical stresses in the presence of a large magnetostriction constant is sufficient to form radial domains.

Inside the microwire are large cylindrical domains, the so-called „cores“, magnetized along the axis of the microwire, as well as a surface annular layer consisting of smaller domains, the direction of the magnetic moment of which depends on the magnetostriction [17]. Amorphous alloys have residual internal stresses in the initial state with a complex inhomogeneous distribution. Due to magnetostriction, the field of internal stress distribution leads to the formation of a complex magnetic (domain) structure [17]. The presence of areas with dark and light contrasts of different intensity (Figure 10, a) indicates that here the radial component of the magnetic moment forms a solid angle with the axis of the microwire. An increase of the external field enhances the contrast of small surface domains (Figure 10, a). This is attributable to the rotation of the magnetic moments of the surface domains during the magnetization [17]. It was determined in Ref. [17] that the axial component of the magnetic moment vector of the surface domain should be oriented in the opposite direction with respect to the axial

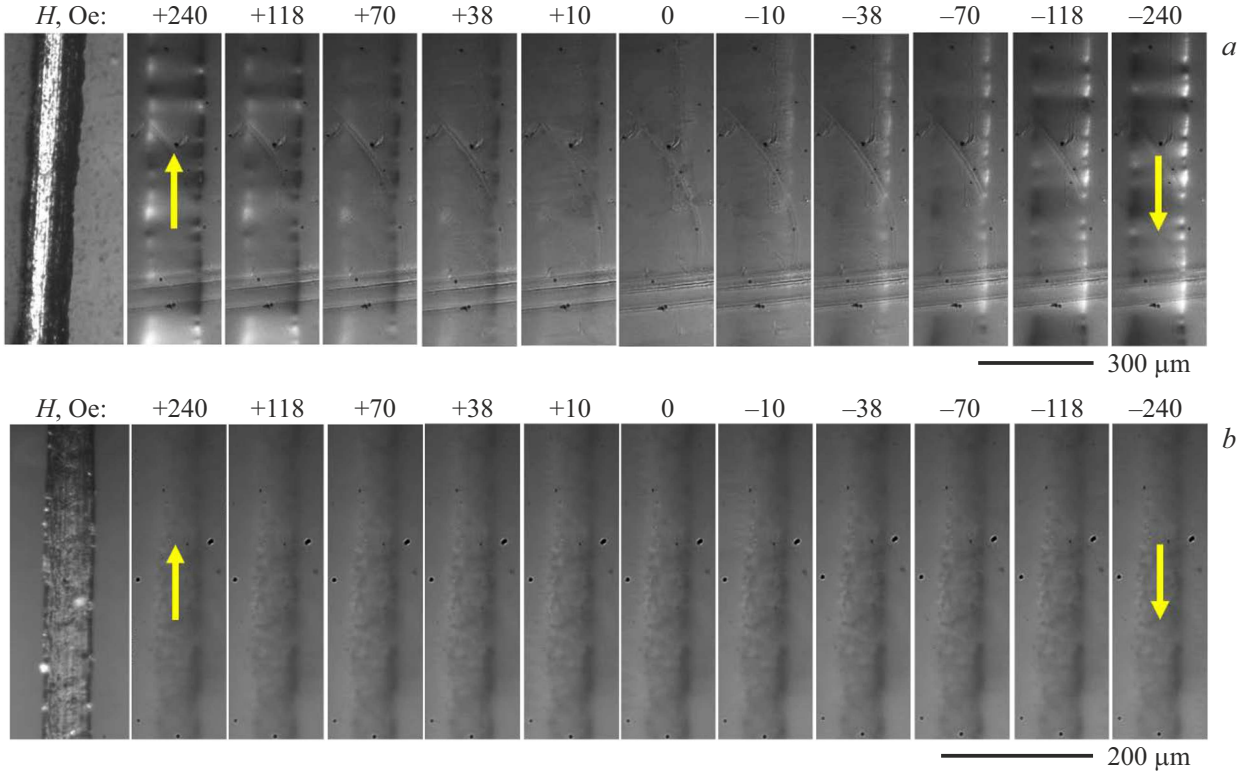

Figure 10. MOIF images in various external fields with the orientation of the field along the axis of the microwire before (*a*) and after (*b*) vacuum annealing. The first photos in the series — optical images of microwires in a microscope. The yellow arrows schematically show the direction of the external magnetic field.

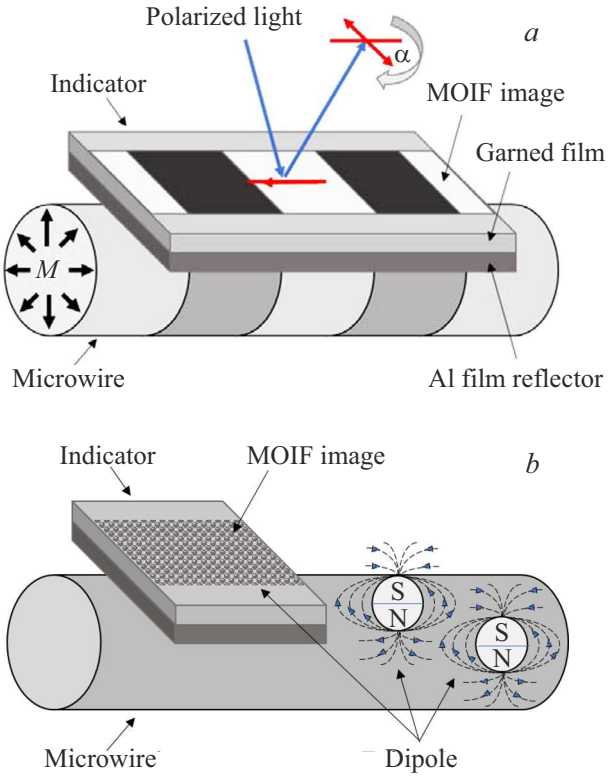

Figure 11. Schematic representation of the magnetization distribution in microwires before (*a*) and after (*b*) vacuum annealing.

component of the magnetic moment of the core domain. Only such a mutual orientation of the magnetization of the surface and large cylindrical domains inside the wire makes it possible to observe an increase of the contrast of small surface domains under these magnetization conditions [17].

4. Conclusions

1. Vacuum annealing of amorphous DyPr–FeCo–B microwires causes the formation of a polycrystalline structure with two main phases: magnetically rigid tetragonal phase $(Pr,Dy)_2(Fe,Co)_{14}B_1$ and magnetically soft phases with a volume-centered iron-cobalt lattice.

2. Heat treatment of microwires causes a significant increase of the coercive force from 8 Oe in amorphous microwires to 10 kOe in polycrystalline microwires, as well as the disappearance of surface radial domains, which are observed in completely amorphous microwires, and also initiates the appearance of a large number of randomly located magnetic dipoles over the entire surface of the polycrystalline microwire.

Funding

The study was carried out within the framework of the state assignment of the Federal Research Center for

Problems of Chemical Physics and Medical Chemistry of the Russian Academy of Sciences 124013100858-3.

Conflict of interest

The authors declare that they have no conflict of interest.

References

[1] A. Gemelli, M. Tambussi, S. Fusetto, A. Aprile, E. Moisello, E. Bonizzoni, P. Malcovati. Micromachines **14**, *4*, 847 (2023).
[2] Md I. Hossain, Md S. Zahid, M.A. Chowdhury, M. Md M. Hossain, N. Hossain. RINENG **19**, 101264 (2023).
[3] S. Büttgenbach, M. Feldmann. IFAC Proc. Vol. **41**, *2*, 12757 (2008).
[4] M. Imboden, J. Morrison, E. Lowell, Han Han, D.J. Bishop. JMEMS **23**, *5*, 1063 (2014).
[5] G. Zhou, Z.H. Lim, Y. Qi, F.S. Chau, G. Zhou. Int. J. Optomechatronics **15**, *1*, 61 (2021).
[6] S. Schonhardt, J.G. Korvink, J. Mohr, U. Hollenbach, U. Wallrabe. IEEE 21st International Conference on Micro Electro Mechanical Systems 479 (2008).
[7] K. Fischer H. Guckel. Microsyst. Technol. **4**, *4*, 180 (1998).
[8] H. Chen, Y. Li, Z. Zhang, S. Wang. Biomicrofluidics **14**, *4*, 041502 (2020).
[9] N. Xia, T.P. Hunt, B.T. Mayers, E. Alsberg, G.M. Whitesides, R.M. Westervelt, D.E. Ingber. Biomed. Microdevices **8**, *4*, 299 (2006).
[10] O.V. Koplak, R.B. Morgunov. Mater. Sci. Eng. B **263**, 114845 (2020).
[11] A. Janutka, P. Gawroski. IEEE Trans. Magn. **51**, *5*, 1 (2015).
[12] O. Koplak, R. Morgunov, I. Khodos. Mater. Lett. **301**, 130291 (2021).
[13] R.B. Morgunov, O.V. Koplak, V.P. Piskorskii, D.V. Korolev, R.A. Valeev, A.D. Talantsev. J. Magn. Magn. Mat. **497**, *1*, 166004 (2020).
[14] R. Morgunov, O. Koplak. Mater. Lett. **273**, 127954 (2020).
[15] Yu. Kabanov, A. Zhukov, V. Zhukova, J. Gonzalez. Appl. Phys. Lett. **87**, 142507 (2005).
[16] O. Koplak, E. Dvoretskaya, M. Stepanov, A. Karabulin, V. Matyushenko, R. Morgunov. Magnetochemistry **7**, *10*, 139 (2021).
[17] N.N. Orlova, A.S. Aronin, S.I. Bozhko, Yu.P. Kabanov, V.S. Gornakov. J. Appl. Phys. **111**, 073906 (2012).

Translated by A.Akhtyamov